Available online at www.sciencedirect.com
SCIENCE DIRECT®
Medical Image Analysis 9 (2005) 237–254
MEDICAL IMAGE ANALYSIS
www.elsevier.com/locate/media

Thoracic non-rigid registration combining self-organizing maps and radial basis functions

George K. Matsopoulos [a,*], Nikolaos A. Mouravliansky [a], Pantelis A. Asvestas [a], Konstantinos K. Delibasis [a], Vassilis Kouloulias [b]

[a] *Institute of Communications and Computer Systems, National Technical University of Athens, 9, Iroon Polytechniou Street, Zografos, Athens 157 80, Greece*
[b] *Department of Radiology, Areteion Hospital, Medical School, University of Athens, Greece*

Received 2 September 2003; received in revised form 21 April 2004; accepted 21 September 2004
Available online 30 December 2004

Abstract

An automatic three-dimensional non-rigid registration scheme is proposed in this paper and applied to thoracic computed tomography (CT) data of patients with stage III non-small cell lung cancer (NSCLC). According to the registration scheme, initially anatomical set of points such as the vertebral spine, the ribs, and shoulder blades are automatically segmented slice by slice from the two CT scans of the same patient in order to serve as interpolant points. Based on these extracted features, a rigid-body transformation is then applied to provide a pre-registration of the data. To establish correspondence between the feature points, the novel application of the self-organizing maps (SOMs) is adopted. In particular, the automatic correspondence of the interpolant points is based on the initialization of the Kohonen neural network model capable to identify 500 corresponding pairs of points approximately in the two CT sets. Then, radial basis functions (RBFs) using the shifted log function is subsequently employed for elastic warping of the image volume, using the correspondence between the interpolant points, as obtained in the previous phase. Quantitative and qualitative results are also presented to validate the performance of the proposed elastic registration scheme resulting in an alignment error of 6 mm, on average, over 15 CT paired datasets. Finally, changes of the tumor volume in respect to each reference dataset are estimated for all patients, which indicate inspiration and/or movement of the patient during acquisition of the data. Thus, the practical implementation of this scheme could provide estimations of lung tumor volumes during radiotherapy treatment planning.

Keywords: Computed tomography; Stage III non-small cell lung cancer; Non-rigid registration; Self-organizing maps; Kohonen neural network; Radial basis functions

1. Introduction

Lung cancer, the most preventable of all human cancers, remains the leading cause of cancer death for both sexes in 2003 (Jemal et al., 2003). Almost one-third of the cancer deaths in men, and almost one-quarter of the cancer deaths in women, are due to lung cancer alone (National Cancer Institute, 1994). The four major types of lung cancer described by the World Health Organization classification are small cell lung cancer (25% of lung cancer), adenocarcinoma (30%), squamous cell carcinoma (25%), and large cell carcinoma (15%) (The World Health Organization, 1982). The last three types are grouped as non-small cell lung cancers (NSCLC) and they have been further categorized in different stages (from Stage 0 to Stage IV), depending on

* Corresponding author. Tel.: +30 210 7722288/1 7722285; fax: +30 210 7223557/1 7723557.
E-mail address: gmatso@esd.ece.ntua.gr (G.K. Matsopoulos).

1361-8415/$ - see front matter © 2004 Elsevier B.V. All rights reserved.
doi:10.1016/j.media.2004.09.002

the progression of the cancer. Specifically, in Stage III, NSCLC tumors have been spread beyond the lung to the chest wall, the diaphragm, or further to the lymph nodes (Oie and Gazdar, 1996).

Computed tomography (CT) is the primary imaging modality for the investigation of lung tumors and the evaluation of various therapeutic schemes applied during staging, including radiotherapy treatment (Burns et al., 2004). Radiotherapy has become widely accepted modality for lung cancer treatment (Lagerwaard et al., 2001) that uses high-energy ionizing radiation (e.g. γ-rays) to kill cancer lung cells. Throughout multiple radiation beams, the radiation is delivered to the treatment area defined by a CT planning software system capable to visualize and reconstruct the tumor and the surrounding lung tissues in three dimensions. Even though the radiation beams are closely focused to tumor treatment area, a number of geometric errors in radiotherapy treatment planning and delivery may be introduced. Such errors may arise from external setup deviations at the treatment unit or from tumor movement within the patient. The former may be minimized by the use of off-line setup correction protocols (de Boer et al., 2001), but the mobility of lung tumors because of the respiration and cardiac action continues to pose a formidable problem (Lagerwaard et al., 2001; Engelsman et al., 2001). Lung tumors motion has been found to be as much as 25 mm near the diaphragm, decreasing in magnitude but increasing in complexity in the middle and upper lobes (Kubo and Hill, 1996). If nothing is done to control or compensate the motion, then the dosimetry margins will be extended beyond the tumor boundary, limiting the intensity of radiation and harming healthy tissue (Murphy et al., 2002).

Several lung motion correction strategies have been documented including multiple slow CT scans (Lagerwaard et al., 2001), breath-holding (Murphy et al., 2002), or combination of breath-holding with external fiducials implanted directly in the lung (Murphy et al., 2003). Also, fast helical CT scanners have been used acquiring images at 0.3 s in one rotation in conjunction with breath-holding (Ross et al., 1990). Although these approaches may stabilize the lung motions up to a certain level, they much depend on the clinical protocol followed at the acquisition of the CT scans. In order to generate a reliable three-dimensional (3D) lung tumor target volume of a patient at different radiotherapy treatment sessions, an a posteriori processing of the CT lung scans based on registration techniques may assist the radiologists to calculate differences in tumor volumes at different times and to design an effective thoracic radiation therapy scheme in terms of dose delivery.

The problem of medical image registration has been extensively addressed in the literature. Comprehensive surveys can be found in (Maintz and Viergever, 1998; Audette et al., 2000). Most of these algorithms have been focused to register brain images with the assumption that they are rigid. In those cases, rigid transformations can only correct translation and rotational differences. Thus, non-rigid transformations are required. An example is the affine transformation, which in addition to rigid mappings allows for scaling and shear (Matsopoulos et al., 2001). Another class of non-rigid transformations is the elastic transformations in which images are considered as continuous bodies and geometric differences are modeled as a result of elastic deformation (Rohr, 2000).

A survey on elastic registration methods for medical images with emphasis on landmark-based schemes has been published by Rohr (2000). According to this class of algorithms, 3D corresponding point landmarks, either fiducial markers placed on the body or anatomical point landmarks localized manually or automatically by applying image operators (Rohr et al., 2003) were initially extracted in both CT-MRI brain data and subsequently input into the thin-plate spline (TPS) deformation model (Bookstein, 1989). Given the displacements of point landmarks, the TPS model interpolates them while minimizing the bending energy of a thin plate, which represents those displacements, by solving a set of linear equations. This approach may yield minimal bending energy properties measured over the whole image, but the deformation is not limited to regions where the common structures are identified (Arad et al., 1994). To cope with local deformations, radial basis functions have been employed in small localized regions in mammographic images (Behrenbruch et al., 2003) and brain tumor in 3D MR dataset (Fornefett et al., 2001). A concise description of techniques for image warping and morphing, including the application of thin plate splines and radial basis functions can be found in (Wolberg, 1998). Furthermore, an algorithm for the non-rigid registration of 3D contrast-enhanced breast MRI was proposed, which combines the normalized mutual information similarity measures with an affine transformation to model the global motion of the breast while the local breast motion is described by a free-form deformation based on B-splines (Rueckert et al., 1999). Recently, landmark- and intensity-based consistent image registration techniques have been presented. Magnotta et al. (2003) proposed an inverse-consistent linear elastic registration algorithm for the alignment of brain MR data, comprising of two phases: the registration of manually identified landmarks to serve for an initial global registration and the matching of intensities and binary segmentation information to refine the registration locally. Similarly, a landmark- and intensity-based consistent image registration algorithm was developed for inter-subject lung registration (Li et al., 2003). Branch points of the pulmonary airway tree were used as internal landmarks, and surface shape information was

based on the 3D boundaries of the segmented lungs. The combination of landmark and intensity information as proposed in the two aforementioned methodologies may result a more biologically meaningful correspondences than traditional unidirectional registration algorithms but they require human intervention by an expert and high execution time (approximately 2 h to register two image volumes), which makes the implementation of these algorithms very difficult on a clinical environment. The non-rigid registration scheme proposed in this paper aims to overcome the aforementioned drawbacks by firstly introducing anatomical features for point correspondence that are automatically segmented from the CT datasets, and secondly by implementing an elastic registration model based on local Radial Basis Functions which results in low execution time applicable to a clinical setting.

A number of registration algorithms have focused on the alignment of thoracic images. These algorithms differ with respect to the image features used as well as the class of the transformations applied. The former includes anatomical features such as bifurcation of pulmonary vasculature (Gee et al., 2003), sternum, vertebrae and trachea (Betke et al., 2003), nodules (Betke et al., 2003; Shen et al., 2002; Brown et al., 2001), lung surfaces and airways (Betke et al., 2003; Kubo et al., 2001; Li et al., 2003; Fan et al., 2001), which were detected either manually or automatically and were used to guide the registration process. The transformations applied to thoracic registration can be broadly classified into rigid and non-rigid transformations. An automatic system for registering CT images of the chest was based on the detection of specific landmarks to provide an initial registration followed by a surface-based rigid registration method using an iterative closest-point (ICP) process (Betke et al., 2003). Of 58 nodules in 10 patients, correspondence was correctly established for 56 nodules (97%). For detection and registration of nodules in chest CT, Brown et al. (2001) developed a rule-based system using fuzzy logic that creates patient-specific models. Also, Kubo et al. (2001) used landmarks and the lung surfaces to register slice-by-slice the CT data using the rigid transformation model. Shen et al. (2002) used a two steps registration method to register CT scans; globally by the use a linear transformation model which includes scaling and shifting in the z-direction and shifts in the x- and y-directions, applied on cross-sectional lung area, and then locally by an ROI-based correlation method. They reported an average nodule mismatch error of only 2 mm. A non-rigid transformation was also implemented towards the establishment of a normative atlas of the human lung (Li et al., 2003) in which segmented lung surfaces are initially aligned using the rigid transformation followed by an intensity-based deformation model over segmented airway trees. A 3D warping model was proposed by Fan et al. (2001) and applied to CT lung images obtained at different stages of breathing. According to this model, a sparse comprehensive displacement field was obtained using airway trees, vessels and lung surfaces as a priori knowledge of the lung deformation, and it was then interpolated over the entire volume iteratively governed by a model derived from continuum mechanics and 3D optical flow. Furthermore, chest CT images were matched with the corresponding PET images (Cai et al., 1999) and PET images with MR images (Makela et al., 2001) using a surface-based registration scheme based on the rigid transformation.

In this paper, a general non-rigid registration scheme is proposed and applied on thoracic CT data acquired at different periods of radiotherapy treatment sessions. The scheme is comprised of four main steps. In the first step, anatomical surface points are automatically extracted from the two data sets, in order to serve as interpolant points. Usually, lung surfaces and/or nodules have been selected for the registration of lung images in the majority of the aforementioned papers (Betke et al., 2003; Kubo et al., 2001; Li et al., 2003; Fan et al., 2001). In our approach, the vertebral spine, the ribs, and shoulder blades are finally selected as candidate points for the registration, since they are easily distinguished from the surrounding tissues, they are uniformly distributed within the whole image data and more importantly, they are bone structures with relative fixed position with the chest in comparison to the lung surfaces used by other researchers. A global pre-registration over the points of the spine vertebra is performed in the next step using rigid transformation in conjunction with the Powell method (Press et al., 1993).

In the third step, an automatic correspondence between sets of points of the vertebral spine, the shoulder blades and the ribs is obtained by the novel application of self-organizing maps (SOMs) (Kohonen, 1982). The automatic determination of point correspondence is a known problem in the literature. Guest et al. (2001) applied a new correspondence calculation algorithm, called correspondence by sensitivity to movement, by determining the sensitivity of a correspondence to movement of the point being matched. Carcassoni and Hancock (2001) investigated the correspondence matching of point sets, using spectral graph analysis. Mayoral and Pérez-Ilzarbe (2000) employed a Hopfield algorithm that favors unicity of the matches for all interest points both on the left and right images in stereo vision. Betke et al. (2003) used an ICP process to determine an automatic point-to-point correspondence between lung surfaces. Our approach towards automatic point correspondence is based on SOMs, expanding the idea described in (Fritzke, 1995; Camp et al., 1998) for surface triangulation. A SOM is an unsupervised competitive

learning neural network that uses lateral neural interaction to discover the topological structure hidden in the data, for visual display in one or two-dimensional (2D) space (Kohonen, 1989). SOMs have been widely used for the clustering of complicated patterns of neural response and unknown fMRI responses (Wismuller et al., 2004), clustering of disc space narrowing grade assignment from cervical X-ray images (Chamarthy et al., 2004), clustering of gene expression data (Huang et al., 2003), clustering breast cancer data in a database (Markey et al., 2003), and segmentation of ophthalmologic MR images using a learning mechanism (Lin et al., 2003).

In the fourth step, a 3D deformation model, based on the radial basis functions (RBFs), is finally applied to the whole volume of the tomographic data, given the displacement of the interpolant points produced by the previous step. Local RBFs have been selected as the deformation model, since they can prevent deformations in regions where no changes are desired, in contrast to the TPS approach which fails to recover local deformations since it yields an overall smooth deformation of the data (Fornefett et al., 2001). The deformation model is based on the implementation of the shifted log function, proposed by Arad et al. (1994) and its underlying mathematical theory for the particular implementation is presented. Since our methodology does not incorporate changes in the attenuation of tissues within the data, no attempt was made towards the application of an intensity-based deformation model to recover deformations, as proposed by Li et al. (2003).

The proposed non-rigid registration scheme is also compared to a surface-based registration method using a rigid transformation in order to evaluate the performance of the two methodologies. Finally, the lung tumor volumes of 15 patients are calculated, with and without the application of the proposed registration scheme and differences of the tumor volumes for all patients are recorded.

2. The non-rigid registration scheme

The proposed non-rigid scheme for thoracic registration comprises of four main steps and it is shown in the block diagram of Fig. 1. Continuous lines indicate control flow, whereas dotted lines indicate data flow between modules. Data flow is indicated as input to the SOM module, since in this case it does not coincide with control flow. According to the block diagram in Fig. 1, 3D anatomical sets of points are initially extracted on the two CT datasets (see Section 2.1). These sets of points correspond to the vertebral spine, the thoracic rib and the shoulder blade contours and they are supersets of the interpolant points. A rigid transformation, in conjunction with Powell optimization technique, is then applied over the vertebral spine points to perform an initial pre-registration of the two CT datasets. Two sets of points are defined, S_2 is the set of points of the vertebrae, ribs and blades, segmented from the reference data and S_1 the set of points of the same anatomical structures from the second dataset, called float data. Preregistration takes place between these sets of points and triangulation of S_1 is performed, before automatic correspondence between them could be determined using a SOM (see Section 2.2). After adaptation, the SOM network results in discovering the pairs of interpolant points, which are further refined by a distance criterion. Finally, RBFs based on the shifted log function, are subsequently employed for elastic warping of the image volume, using the correspondence between the interpolant points, as obtained in the previous step (see Section 2.3).

2.1. Detection of anatomical features

In the first step of our approach, anatomical features are extracted from the CT datasets, the reference and the float datasets. As anatomical features, the vertebral spine, the thoracic ribs, and shoulder blades are finally selected, since they are bone structures, with relative

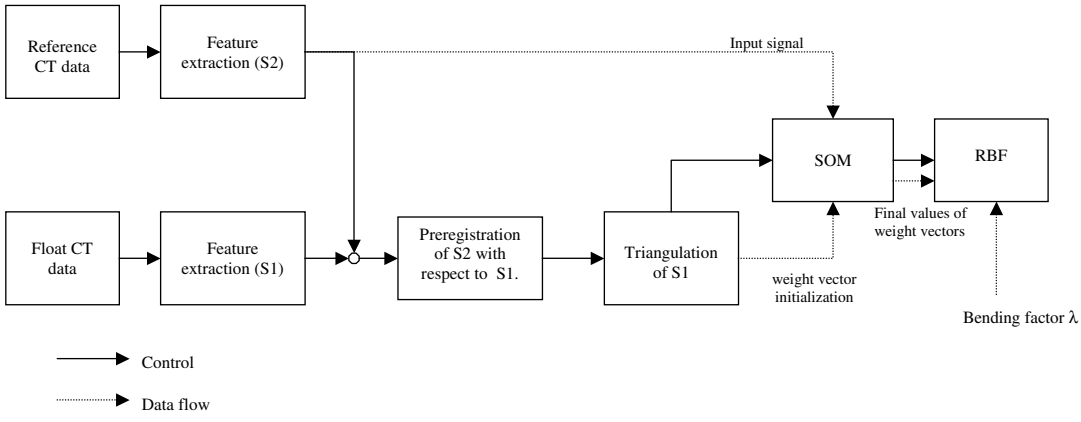

Fig. 1. Block diagram of the proposed elastic registration scheme. Continous lines indicate control flow and dotted lines data flow between modules.

fixed position within the chest and they have attenuation values (>700 Hounsfield units – HU)) that are significantly higher than the surrounding tissues (80–100 HU).

The anatomical features are extracted by a process, which resembles the first step of the algorithm proposed by Hu et al. (2001) for the extraction of lung surfaces. According to our extraction process, an initial threshold is applied in an iterative way that separates voxels of low-density corresponding to air and/or other areas (such as the Gantry, etc.) from the chest body area. The initial threshold is selected based on the CT number for pure air (−1000 HU) and the CT number for voxels within the chest body (around 0 HU). A second iterative thresholding procedure is applied to extract the vertebral spine, the thoracic ribs and shoulder blades from the rest of the chest body. The initial threshold is selected based on the CT number for chest/wall body (approximately 0 HU) and the CT number for voxels within the anatomical features (700 HU). Then, a morphological opening operation defined by: $(I \circ b) = (I \ominus b) \oplus b$, where I is the binary slice containing the segmented anatomical features, $\ominus$ and $\oplus$ denote the morphological operations of erosion and dilation, respectively, and b the structuring element (Serra, 1988), is applied slice by slice to smooth the areas of the anatomical features from bulges of the surrounding tissues and to discard small isolated regions that are present during thresholding. The opening operation is iteratively performed for four times using a cross-structuring element of size 3×3. Finally, a morphological contour algorithm (Matsopoulos and Marshall, 1994) is applied slice by slice to obtain the contour points of all anatomical features.

Lung surfaces have been selected by other researchers as typical anatomical structures for the 3D lung registration (Betke et al., 2003; Li et al., 2003). In the present study, the lung surfaces are excluded as features in the registration scheme since they are not in a relative fixed position due to the occurred deformations and they are difficult to be automatically extracted in cases where lung tumors invade the thoracic wall. Furthermore, lung surfaces were finally segmented only for visualization purposes. Thus, lung surfaces are semi-automatically extracted by applying initially the seeded region growing technique (Adams and Bischof, 1991). Given two seed points, one placed within the left and the other to the right lung regions, the algorithm finds a tessellation of the 3D image into lung regions with the property that each connected component of a region meets exactly each initial seed point. Subject to this constraint, the region is chosen to be as homogeneous as possible. A morphological opening with a 3×3 structuring element is also applied slice by slice to smooth the lung areas. Finally, binary contours of the left and the right lungs are obtained (Matsopoulos and Marshall, 1994). The proposed methodology has failed to segment lung regions in slices where tumors are extended in the left or right lung, attached or invaded to the thoracic wall. In those cases, and since the tumor splits the left or the right lung area in two parts, the larger part of the lung was only segmented by the proposed methodology. In order to recover the other missing part, the aforementioned procedure is repeated by placing a seeded point in the missing lung part. All tumor boundaries are manually defined, in a slice-by-slice basis, by an experienced radiologist, both in the reference and the registered CT datasets for the tumor volume calculations.

2.1.1. Pre-registration process

An initial pre-registration is then performed based on the sets of points that correspond to the spine vertebra obtained by the previous process. The selection for these points is based on the fact that points of the spine vertebra are rigid and remain un-deformed during physiologic movement. The spine vertebra points are extracted from the other segmented anatomical features using an erosion operation followed by the morphological opening by reconstruction of erosion (Zana and Klein, 2001). Initially, morphological erosion is performed to all binary slices in which the vertebrae are connected to the surrounding ribs, with a rectangular structuring element of dimensions 15×1, oriented along the y-axis. This operation results in isolating the required structures from the surrounding bone structures. In the next step, each slice containing the extracted features (ribs, isolated vertebrae and blades) is morphologically filtered by: $I^R_{\text{spines}} = (I \circ B_R) \circ_{\text{rec}} I$, where I is the original binary slice, B_R is a circular binary structuring element with radius $R = 20$ pixels, $\circ$ is the morphological opening operation and $\circ_{\text{rec}}$ is the operation of the opening by reconstruction of erosion. Initially, the original slice is processed by a morphological opening operation, which results in the removal of regions with size less or equal to the size of the structuring element used, typically the spine vertebra. Then, the operation of opening by reconstruction of erosion is applied which reconstructs only the removed regions from the application of the opening operation.

The pre-registration process is applied in three dimensions. The coordinate system is defined as follows: the x-axis corresponds from left to right, the y-axis from back to front whereas the z-axis from head to feet (cranio-caudal direction). The pre-registration is then performed using the rigid transformation in conjunction with the Powell method (Press et al., 1993), as an optimization technique (Matsopoulos et al., 2003). The final step of the pre-registration consisted of the production of the distance map (DM) from the reference set of the corresponding 3D points. The DM a discrete space in which each voxel holds a value equal to its Euclidean distance from the closest node of the reference set of surface points (Kozinska et al., 1997). The DM accelerates

the process of matching the reference and float sets consisting of N nodes each, since it reduces the problem's complexity from $O(N^2)$ to $O(N)$. The pre-registration process is applied in order to realign the two datasets in all coordinates.

2.2. Automatic definition of correspondent points based on SOMs

In this section, an overview of SOMs and the automatic correspondence of the sets points by initializing the Kohonen model are analytically presented.

2.2.1. Self-organizing maps: an overview

SOM is a neural network, which uses a competitive learning algorithm to train itself in an unsupervised manner. Kohonen first established the relevant theory and explored possible applications (Kohonen, 1982). The Kohonen model comprises of a 2D layer of neurons m. Each neuron is fed by input vector (data point) $\vec{x} \in \Re^n$ through a weight vector $\vec{w} \in \Re^n$. Each time a data point is input to the network, only the neuron j whose weight vector resembles most the input vector, is selected to fire, according to the following rule:

$$j = \arg\min_{i=1}^{m}(|| \vec{x} - \vec{w}_i || ^2). \quad (1)$$

The firing or winning neuron j and its neighboring neurons i have their weight vectors $\vec{w}$ modified according to the following rule:

$$\vec{w}_i(t+1) = \vec{w}_i(t) + h_{ij}(|| \vec{r}_i - \vec{r}_j ||, t)(\vec{x}(t) - \vec{w}_i(t)), \quad (2)$$

where $h_{ij}(|| \vec{r}_i - \vec{r}_j ||, t)$ is a kernel defined on the neural network space as a function of the distance $(|| \vec{r}_i - \vec{r}_j ||)$ between the firing neuron j and its neighboring neurons i, as well as the time, defined as the number of iterations t. This kernel has the approximate shape of the "Mexican hat" function, which, in its discrete form, has maximum value at the position of the winning neuron, whereas its value drops in a Gaussian manner as the distance from the winning neuron increases. The width of this function decreases monotonically with time t. In this way, convergence to the global optimum is attempted during the early phases of the self-training process, whereas gradually the convergence becomes more local as the size of the kernel decreases. Each time a new signal is fed into the network, the neurons compete and the one with the weight vector closest to the signal, according to Eq. (1) is selected to fire. The firing neuron adjusts its weight vector so that it matches even better with the incoming signal. Its neighboring neurons modify their weight vectors so they also resemble the input signal, but less strongly, depending on their distance from the winner. This learning mechanism is completely defined by the $h(|| \vec{r}_i - \vec{r}_j ||, t)$ kernel, as it has been described above.

2.2.2. Point correspondence based on the Kohonen model

Triangulation of sets of surface points based on Kohonen model: The objective of this step is the triangulation of the sets of points corresponding to the contours of vertebrae, ribs and blades, in both datasets. Let S_2 be the set of anatomical points in three dimensions of the reference data, whereas S_1 the set of points of the same anatomical structures from the float data (after the application of the pre-registration process).

The network firstly triangulates these two sets. Fritzke (1995) originally introduced 2D triangulation using SOMs and a class of similar techniques with or without fixed network dimensionality, based on competitive learning. Also, Camp et al. (1998) applied Fritzke's work to reconstruct 3D medical data towards virtual reality applications. Neither of the two research works introduced a direct application to 3D data registration. Based on the Fritzke's work, the triangulation is performed by defining a SOM with the following characteristics:

- The size of a rectangular grid of neurons $N_1 \times N_2$ is set to a desirable value that covers the characteristic dimensions of the points of the sets S_1 and S_2, capable to capture the details of the two datasets. Considering the above, a grid of neurons of 20 rows by 100 columns (20×100) is chosen for the specific implementation.
- The initial weighting vectors of the neurons of the grid are set equal to the coordinates to a set of points of an enclosing surface with the same topology with the surface that is to be triangulated, typically a cylindrical surface.
- The input to the neural network consists of the Cartesian coordinates of the set of points that need to be triangulated. This process is only necessary for the float data S_1.

After the process of adaptation of the neural network, the weighting vectors of the neurons have values identical to the appropriate points of S_1. A wire frame consisting of one node for each neuron can be constructed, with Cartesian coordinates of each node equal to the weight vector of the corresponding neuron. The wire frame is triangulated due to the connectivity of the neurons, while its nodes closely follow the set of points to be triangulated, because of the neural network adaptation process.

Automatic definition of corresponding points: The search for corresponding points is based on the concept of replicating the topology of the set S_1 (set of candidate anatomical points of the float image) on the input layer of a SOM model. One neuron is assigned to each node of the float set. The connections between the neurons are identical with the connections of the wire frame (lattice) of the float set. No connection between two neu-

rons is allowed if the two corresponding nodes are not directly connected on the float set. The initial weight vector of the neurons, according to Eq. (2), is the Cartesian co-ordinates of the corresponding wire frame nodes in the 3D space – $\vec{w} \in \Re^3$ – as described in the previous subsection.

The training of the network is performed by presenting the network with the coordinates of randomly selected points sampled from the reference set, S_2 (set of candidate set of points of the reference image). The kernel that controls the learning rate of the network is defined as follows. The spatial part consists of a Gaussian function of the Euclidean distance $d_{rq} = ||r-q||$ between the winner neuron r and the neighboring one, q. This kernel is formulated as follows:

$$h_{rq}(||\, r-q\, ||, t) = h_{rq}(d_{rq}, t) = \varepsilon_i \left(\frac{\varepsilon_f}{\varepsilon_i}\right)^{t/t_{max}} e^{-\frac{d_{rq}}{\sigma^2(t)}}, \quad (3)$$

where ε_i and ε_f are positive initial and final parameters defined experimentally and t_{max} corresponds to the maximum number of iterations. The standard deviation $\sigma(t)$ of the Gaussian is defined as: $\sigma(t) = \sigma_i(\sigma_f/\sigma_i)^{t/t_{max}}$, where σ_i and σ_f are the initial and final values of $\sigma(t)$.

The lateral interactions between the winning and the neighboring neurons, as defined by Eqs. (2) and (3), are confined to a window of size 3×3 of neurons throughout the network training (see Section 4 of the discussion for details of the selection of the window size). The definition of the distance function d_{rq} between the two neurons r and q is defined as Manhattan distance (the sum of the absolute differences of the neuron coordinates) within the 3×3 neuron neighborhood. To ensure that the deformed float set, produced by the weight vectors of the SOM network, is closed at the vertical boundary neurons of the orthogonal grid, it is essential that these neurons must interact with each other. Therefore, the definition of a 3×3 neighborhood around a boundary neuron is modified so that it wraps around the vertical boundary. This is demonstrated for a particular case in Fig. 2, where the winning neuron in the first column of the lattice, shown in black, is surrounded by a 3×3 neighborhood of neurons shown in gray. The displayed lattice of neurons is reduced to 16×20 for visualization purposes.

The convergence of the SOM network during the triangulation of the S_1 set of points results in a triangulated subset of points (S_1'), with a number of points equal to the number of nodes of the triangulated set – typically 2000 points. Each node of subset S_1' corresponds to a neuron of the SOM network, whose initial weighting vector (x_0,y_0,z_0) of S_1 is equal to the initial Cartesian coordinates of this node. In the deformed subset (after SOM adaptation for automatic definition of corresponding points), this node is displaced to new coordinates, equal to the final weighting vector (x_1,y_1,z_1). The new position always coincides with a point of the reference set, S_2. The points (x_0,y_0,z_0) and (x_1,y_1,z_1) constitute a pair of interpolant points. Despite the fact that SOM lateral interactions between neurons cause a one to one point correspondence, there is no way to prohibit rare cases in which more than one points from S_1' correspond to one point of S_2. However, most such point mismatches are discarded by the application of a distance threshold criterion that excludes corresponding points that they exceed a distance more than five voxels. This process also prohibits excessive deformation of the final warped image. Thus, the total number of successful corresponding points is reduced to approximately 500 pairs of points for all patient data (for more details on the selection of this number of pairs of points see Section 3).

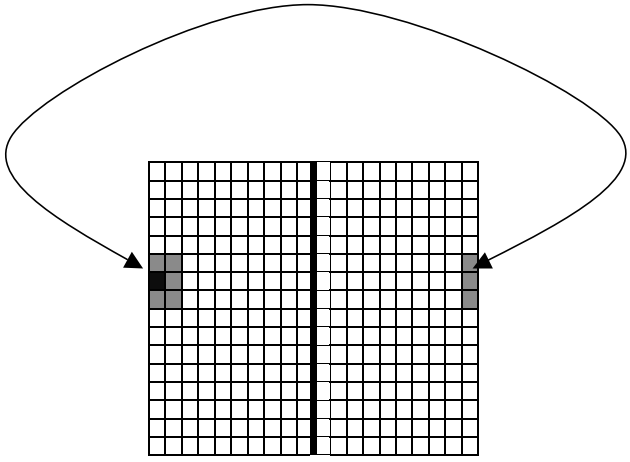

Fig. 2. Neighborhood definition (grey areas) round the winning neuron (black square) shown graphically in a 16×20 lattice of neurons.

2.3. The 3D warping method

2.3.1. Mathematical definition of the warping method

The elastic deformation of the 3D lung transformed image with respect to the corresponding lung reference image, is based on the calculation of a displacement Field (F) function, defined over the volume of the transformed image, which will be deformed. A displacement Field (F) is a 3D vector function which assigns a spatial displacement $\delta\vec{r}$ to each of the transformed image voxels (x,y,z):

$$F(\vec{r}) = F(x,y,z) = \delta\vec{r}(x,y,z). \quad (4)$$

The value of the F function is known for each position $\vec{r}_{ij}$ of the points of the wire frame (interpolant points) of the float image, prior to deformation. The coordinates of the interpolant points coincide with the initial weighting vector of the neurons of the SOM network. The value of the F function is defined according to the following equation:

$$F(\vec{r}_{ij}) = \vec{w}_{ij} - \vec{r}_{ij}, \quad \text{for } i = 1,\ldots,N_1 \text{ and } j = 1,\ldots,N_2, \quad (5)$$

where $\vec{w}_{ij}$ is the final value of the weighting vector of the (i,j) neuron calculated by the Kohonen network. The problem of 3D image registration is equivalent to calculating the F function for every voxel of the image, prior to deformation. The calculation of the F, as a function of spatial position, given its value at specific positions, indicates a problem of multivariate interpolation. Assuming the RBF interpolation method, the value of the displacement field at any position $\vec{r}(x,y,z)$ of the transformed image volume is given by

$$F(\vec{r}) = \sum_{i=1}^{N_1}\sum_{j=1}^{N_2} \vec{a}_m g(\| \vec{r} - \vec{r}_{ij} \|) + p(\vec{r}), \tag{6}$$

where $g : \Re^+ \to \Re$ is a univariate function, m is a "dummy variable" defined as $m = m(i,j) = (j-1)N_1 + i$ and $p(\vec{r}) = \vec{c}_0 + \vec{c}_1 x + \vec{c}_2 y + \vec{c}_3 z$ is a first-degree polynomial which is added because pure radial sums can not realize the affine transformation. $\vec{c}_n = (\vec{c}_n^x, \vec{c}_n^y, \vec{c}_n^z)$, with $n = 0,1,2,3$ and $\vec{a}_m = (a_m^x, a_m^y, a_m^z)$ are the function parameters to be estimated. The definition of Eq. (6) has been proven to be an effective tool for the problem of multivariate interpolation (Arad et al., 1994). The coefficients $\vec{a}_m$ and $\vec{c}_n$ are calculated by solving the three systems of linear equations (one for each Cartesian axis) of size $(M+4)\times(M+4)$, where $M = N_1 \times N_2$:

$$GA_x = F_x, \tag{7a}$$

$$GA_y = F_y, \tag{7b}$$

$$GA_z = F_z, \tag{7c}$$

where matrix $\mathbf{A}$ is defined as $A = (\vec{a}_1, \vec{a}_2, \ldots, \vec{a}_M, \vec{c}_0, \vec{c}_1, \vec{c}_2, \vec{c}_3)^{\mathrm{T}}$, $\vec{a}_m = (a_m^x, a_m^y, a_m^z)$, $m = 1,\ldots,M$ and vectors A_x, A_y, A_z are the first, second and third column of matrix $\mathbf{A}$ respectively. Vectors F_x, F_y, F_z are the first, second and third column of matrix $\mathbf{F}$ respectively, where $F = (F_1, F_2, \ldots, F_M, 0, 0, 0, 0)^{\mathrm{T}}$ and $F_m = (\vec{w}_{ij} - \vec{r}_{ij})$. The indexes i and j and m are connected according to Eq. (7e).

$$G = \begin{bmatrix}
g_{11} & g_{12} & \bullet & \bullet & \bullet & g_{1M} & 1 & x_1 & y_1 & z_1 \\
g_{21} & g_{22} & \bullet & \bullet & \bullet & g_{2M} & 1 & x_2 & y_2 & z_2 \\
\bullet & \bullet & \bullet & \bullet & \bullet & \bullet & \bullet & \bullet & \bullet & \bullet \\
\bullet & \bullet & \bullet & \bullet & \bullet & \bullet & \bullet & \bullet & \bullet & \bullet \\
\bullet & \bullet & \bullet & \bullet & \bullet & \bullet & \bullet & \bullet & \bullet & \bullet \\
g_{M1} & g_{M2} & \bullet & \bullet & \bullet & g_{MM} & 1 & x_M & y_M & z_M \\
1 & 1 & \bullet & \bullet & \bullet & 1 & 0 & 0 & 0 & 0 \\
x_1 & x_2 & \bullet & \bullet & \bullet & x_M & 0 & 0 & 0 & 0 \\
y_1 & y_2 & \bullet & \bullet & \bullet & y_M & 0 & 0 & 0 & 0 \\
z_1 & z_2 & \bullet & \bullet & \bullet & z_M & 0 & 0 & 0 & 0
\end{bmatrix}, \tag{7d}$$

where $g_{mn} = g(\| \vec{r}_{ij} - \vec{r}_{kl} \|)$ with $i,k = 1,\ldots,N_1$ and $j,l = 1,\ldots,N_2$ and $m,n = 1,\ldots,M$. The index m of the element of the G matrix and the indexes i,j of the interpolant points are connected as follow:

$$i = \mathrm{mod}\left(\frac{m-1}{N_1}\right) + 1 \text{ and } j = \mathrm{div}\left(\frac{m-1}{N_1}\right) + 1, \tag{7e}$$

where mod and div are the functions returning the modulus and the integer part of the division of two real numbers. Similar relationships hold for the index n with k and l indexes. The triplet (x_m, y_m, z_m), $m = 1,\ldots,M$ are the Euclidean coordinates of the interpolant point $\vec{r}_{ij}$, where the indexes i and j are calculated according to Eq. (7e).

Several approaches have been reported in the literature for the g-function, for which the three linear systems of Eqs. (7a)–(7c) have a unique solution (Arad et al., 1994). The shifted log function is selected as the g-function, according to the following equation:

$$g(t) = \log(t^2 + c^2)^{\frac{1}{2}} \text{ for } c^2 \geqslant 1 (\text{shifted log}). \tag{8}$$

As it will become clear when the bending factor is introduced, the value for constant c was set to 1, so that the M first elements of the main diagonal of matrix $\mathbf{G}$ are equal to 0.

The F function can be defined according to Eq. (6) for each dimension as follows:

$$F(\vec{r}) = (F_x(\vec{r}), F_y(\vec{r}), F_z(\vec{r})), \tag{9}$$

where

$$F_x(\vec{r}) = \sum_{i=1}^{N_1}\sum_{j=1}^{N_2} a_m^x g(\| \vec{r} - \vec{r}_{ij} \|) + c_0^x + c_1^x x + c_2^x y + c_3^x z, \tag{10}$$

where $m = m(i,j) = (j-1)N_1 + i$. $F_y(\vec{r})$ and $F_z(\vec{r})$ are defined similarly.

In (Arad et al., 1994), a measure of bending energy was defined and a relative parameter was introduced, called bending factor λ, which balances the requirement for exact matching of the interpolant points. The introduction of the bending factor λ requires the $\mathbf{G}$ matrix (Eq. (7d)) to be redefined so that the M first main diagonal elements of matrix G are set to λ: $g_{mm} = \lambda$, $m = 1,\ldots,M$ (thus the requirement for setting $c = 1$).

When the bending factor is zero, $\lambda = 0$, the calculated F results in an exact match of the interpolant points at the expense of a possibly high total spatial bending measurement, of the image space. When λ approaches large positive values, the sum of square distances between actual and calculated positions of the interpolant points is minimized, while the total spatial bending measurement, kept below a threshold value which depends on λ, or equivalently, the geometric transformation approaches the affine one. The value of the bending factor λ is estimated by visual inspection of the deformed image (Rohr et al., 2001). Fig. 3 confirms these arguments for a synthetic grid image, containing six (6) interpolant points

(crossed bullets in the figure). Four interpolant points remain fixed, whereas the other two interpolant points move towards each other, as shown in top left image. The warped images are shown in the top right image and in the two bottom images for increasing values of the bending factor λ corresponding from the pure RBF interpolation method (top right image) to the affine transformation approximation (bottom right image).

2.3.2. Implementation issues of the proposed non-rigid registration scheme

The proposed elastic deformation scheme, based on the SOM adaptation, can be summarized in pseudocode, as follows:

```
Segmentation of the reference data produces a set of surface points, S2
Segmentation of the transformed data produces a set of surface points, S1
Triangulation of S1
Obtain the DM of the set S2
Pre-registration and triangulation of S1 into the coordinate frame of S2
Perform the elastic deformation method, based on the Kohonen model, as follows:
  Sample the set S2 and store the sampled points into a queue Q
  Construct a layer of neurons by assigning one neuron to each node of the triangulated S1 and establish connections of each neuron with its neighbors of the triangulation of S1
Assign an initial weight vector to each neuron, containing the current Euclidean coordinates of the corresponding S1 node
Time = 0
While (time<threshold) do
  Update the network kernel according to Eq. (3)
  Present the network with the coordinates of a random point from queue Q
  Select a winning neuron according to Eq. (1)
  Update the weighting vectors of the winner and its neighbors according to Eq. (2)
  Time = time + 1
```

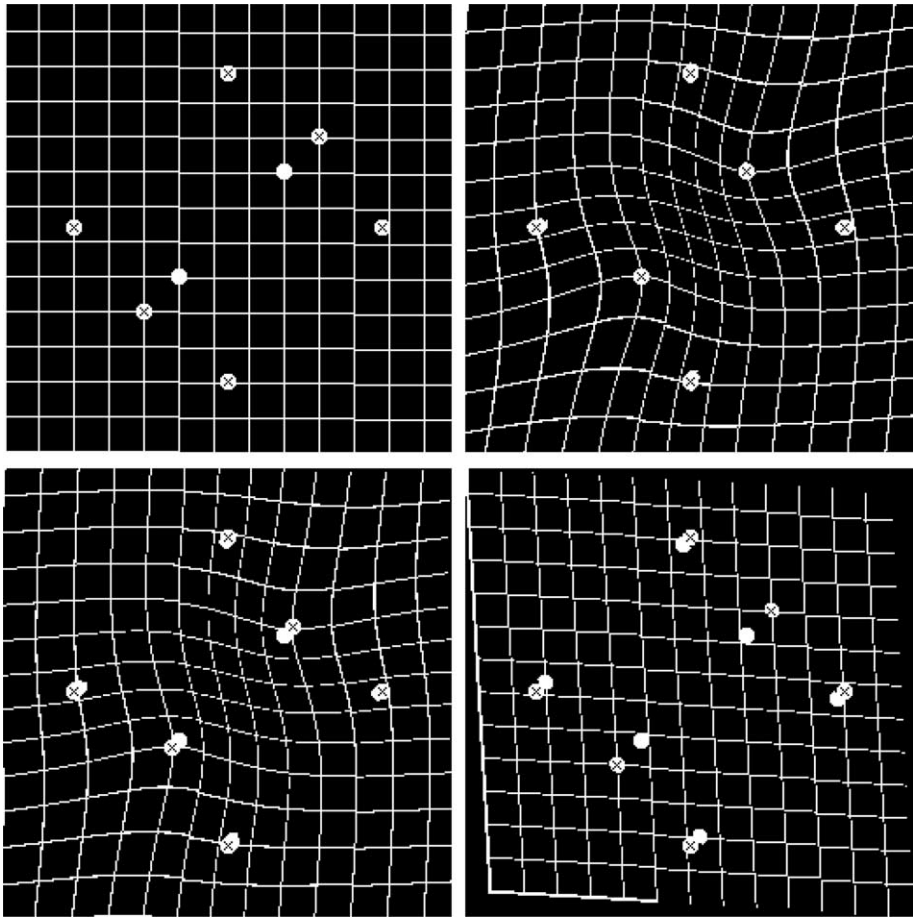

Fig. 3. Effect of the bending factor λ on image warping. Top left: the synthetic grid image showing initial (marked with 'x') and final position of the interpolant points. Top right: for $\lambda = 0.005$. Bottom left: for $\lambda = 0.05$. Bottom right: for $\lambda = 5$ (affine transformation approximation).

```
Set as interpolant points the final and the
initial weight vector of each neuron, for
which the magnitude of the vector differ-
ence is equal to or less than five voxels
in respect to the reference set
Set bending factor λ = 0.05
Calculate the interpolation coefficients,
according to Eq. (7) to define the dis-
placement Field (Eq. (6)) using the g-func-
tion of Eq. (8)
Calculate the displacement Field for every
voxel of the transformed image, according
to Eq. (10), to register the float image to
the reference image
```

The kernel that controls the learning rate of the Kohonen neural network is defined according to Eq. (3) with parameters $\varepsilon_i = 0.5$, $\varepsilon_f = 0.005$, $\sigma_i = 3.0$ and $\sigma_f = 0.1$, for $t_{max} = 50{,}000$ maximum number of iterations and are obtained experimentally for all pairs. These values of the parameters are in accordance to Fritzke (1995). The g-function of Eq. (6) is selected to be the shifted log function, defined in Eq. (8), with $c = 1$. The value of the bending factor λ is selected to be $\lambda = 0.05$, for all data pairs. This experimentally chosen value, in conjunction with the filter that rejects interpolant points whose magnitude of displacement vector is greater than five voxels, was optimal under a qualitative assessment performed by an expert oncologist. Higher values of λ result in a transformation, which resembles the affine, thus loosing the desired property of elasticity, whereas lower values result in a deformation with high measure of the total spatial bending, leading to physically meaningless results. In the later case, deformation may cause the transformed set to be warped so that it matches the reference set, whereas ignoring any anatomic information. This argument is in agreement with the test images displayed in Fig. 3.

3. Results

3.1. Patient data

The inclusion criteria for the patients entering the study were the following: patient with NSCLC histologically proven with Stage III of disease (TNM classification); age ranging from 40 to 60 years; Karnofsky performance status >70 (Movsas et al., 2003). The patients signed a consent form for participating in the study. The study design in clinical terms included two CT scans: one at the baseline of radiotherapy schedule and a second one four weeks thereafter. The patients were treated with radiotherapy in a treatment schedule of six weeks (2 Gy per fraction, five days a week, 60 Gy total dose). Initially, 17 patients were enrolled in the study. However, two patients were excluded from the study. These patients suffered from dyspnoea related to radiation induced pneymonitis and were unable to undergone the second session of CT scan four weeks after the baseline. Thus, their performance status was lower than 70 and they were excluded from the study.

Fifteen (15) patients were finally selected for the present study from the Department of Radiology, Medical School of University of Athens, at the Areteion Hospital. The patients were diagnosed having lung tumors and they were under radiotherapy treatment. For the evaluation of the proposed methodology, the CT image data of each patient at baseline of radiotherapy was selected as a reference image, whereas the CT data at four weeks from the baseline treatment and during the radiation schedule were chosen as transformed data.

For ten (10) of the patients, called Group A, the following protocol was applied: The reference CT data were acquired with instructions given to patients for expiration, according to the specific clinical protocol, since it was a diagnostic CT. No specific instructions were given to the patients in terms of inspiration, during acquisition of the post treatment CT. The CT transformed data were acquired at four weeks from the reference data. For the rest five (5) patients, called Group B, the clinical protocol was modified as follows: No specific instructions were given to the patients in terms of inspiration, during any CT acquisition. This was done in order to evaluate the proposed elastic registration scheme during real conditions in a routine clinical procedure.

In all patients, the lung tumor was more than 3 cm in diameter in the one lobe (left or right), invading the chest wall with metastases to contralateral mediastinal lymphnodes (Stage III). The reproducibility of the patient approximate set-up in the CT gantry was assured to a relative degree of accuracy, by using ink skin markers, resulting from the simulation of the radiation therapy. These markers were not radio-opaque markers and consequently they were not used for image registration.

The patient data were acquired with a multi-helical Philips CT using a 10 mm collimator and were reconstructed in 1.25 mm increments using a high-frequency reconstruction algorithm. The images were acquired with a 512×512 matrix representing the acquired size along the x- and y-axes and were quantized using 12 bits per pixel. The slice thickness was 4 mm with zero slice spacing finally corresponding to the size along the z-axis. All the patient data contained 32 slices. The voxel size of all the data was $0.5 \times 0.5 \times 4.0$ (in mm). Finally, during this study, it was deemed necessary that the CT data covered the whole tumor area with a reasonable margin in the z-direction.

3.2. Elastic registration results

The performance of the proposed elastic registration scheme presented in the previous sections is visually demonstrated in terms of transverse sections. In Fig. 4, the vertebrae, the ribs and the shoulder blade contours for a typical transverse section of the matched images of Patient-11 of Group B are displayed at different phases of the proposed registration. In the top left, the relative position of the extracted anatomical feature contours of the reference slice (white colored contours) and the transformed slice (grey colored contours), at the same z-coordinate, is displayed, before the application of the registration scheme. It must be pointed out that the segmented anatomical features in the corresponding transverse slices of the figure at the same z-coordinate were non-identical due to the different position of the patient before acquisition, the internal motion because the patient was not at the same phase of respiration and the sparse sampling along the z-axis (voxel size along the z-axis of 4 mm). In the top right, the relative potion of these contours is shown after the application of the pre-registration method using the rigid transformation. It can be noticed that even though the points of the spine vertebra are mainly aligned and some minor corrections are made at the cranio-caudal direction, the remaining rib and shoulder blade contours are still unmatched due to the deformation. Finally, the effect of the application of the non-rigid registration scheme can be seen from the relative position of the anatomical contours in the lower image. Any minor mismatches after the application of the non-rigid registration scheme were mainly due to the selection of the bending factor λ of the warping method rather than the correspondence using SOMs.

Fig. 5 demonstrates the effect of the proposed non-rigid registration, based on RBFs, on a number of corresponding interpolant points as defined by the SOM adaptation. Despite the fact that the proposed non-rigid deformation is purely 3D, the effect of elastic transformation is visualized on a randomly selected transform slice of a patient. The top image shows the vertebrae, ribs and blades contours of the reference transverse slice superimposed on the float slice at the same z-coordinate, before non-rigid registration. In the same figure, the corresponding points of the image to be transformed (square marks), whose z-coordinate is equal to the slice coordinate, are shown along with the corresponding points of the reference image (circles). It has to be mentioned that only the pairs of interpolant points that lie exactly on these slices are visualized; although all interpolant points whose z-coordinate has the same integer part with the slice z-coordinate, take part in the calculation of the elastic registration. The lower image of Fig. 5 visualizes the deformed float CT slice at the same z-coordinate with the reference one, after the application of the proposed non-rigid registration scheme. In this case, the vertebrae, ribs and blade contours of the reference slice are correctly

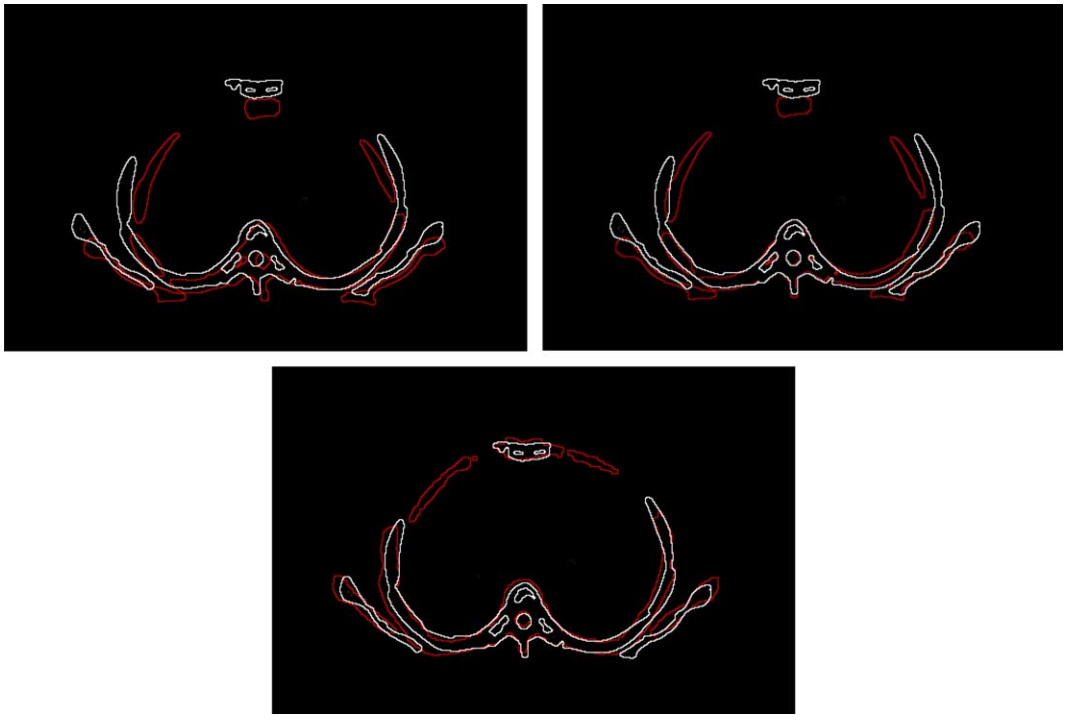

Fig. 4. Performance of the elastic registration scheme for Patient-11 of Group B. Top left: relative position of the extracted feature contours from the reference (white colored contours) and the float (grey colored contours) slices before registration. Top right: relative position of the contours after the application of the rigid registration. Bottom: relative position of the contours after the application of the proposed elastic registration scheme.

matched with the corresponding anatomical features of the deformed slice. The corresponding interpolant points with distance greater than five voxels have not been filtered out for the purposes of the figure. As it can be seen, the pair of interpolant points of the spine vertebra seemed to almost coincide, partly due to the application of the rigid transformation. Also, correspondence has been achieved for the rest interpolant points corresponding to the ribs and blades. Any minor spatial mismatches may be mainly due to the selection of the bending factor used in the warping method.

The performance of the proposed methodology is also shown in Fig. 6 for typical transverse corresponding slices of Patient-11 of Group B, by overlaying the lung contours of the reference data. As it is stated in the previous section, the superimposition of the lung contours was only for purpose of visual assessment. All results were visually inspected and evaluated by clinical radiation oncologists. In the top row of the figure, the reference slice (left image), the corresponding slice to be transformed (middle image) before registration, and the deformed slice (right image), after elastic registration, are displayed. The x- and y-coordinates of the displacement field are visualized in the form of a deformed wire frame, on the right images. It can be seen that the reference lung contours are aligned with the deformed corresponding float slice.

Another pair of corresponding slices of the same patient is displayed in the second row. The lung tumor covers the left lung area and it attaches the thoracic wall as it can be observed in the reference (left image) and float (middle image) slices displayed, respectively. The elastic registration result is shown in the right image, where the majority of the lung contours of the reference slice are aligned with the deformed slice. The displacement field along the x- and y-axes is also visualized. It can also be observed that minor mismatches occurred at the left lung close to the spine below from the area of the tumor. These mismatches were due to the fact that the information input to the warping method originated from the interpolant points based on the spine and the ribs and not from the tumor itself.

The performance of the proposed elastic registration algorithm was also visually assessed in terms of lung tumor surfaces for the case of Patient-1 from Group A. Since the patient diagnosed with Stage III NSCLC, the tumor area is attached to the chest wall, automatic segmentation of these volumes was a difficult task to per-

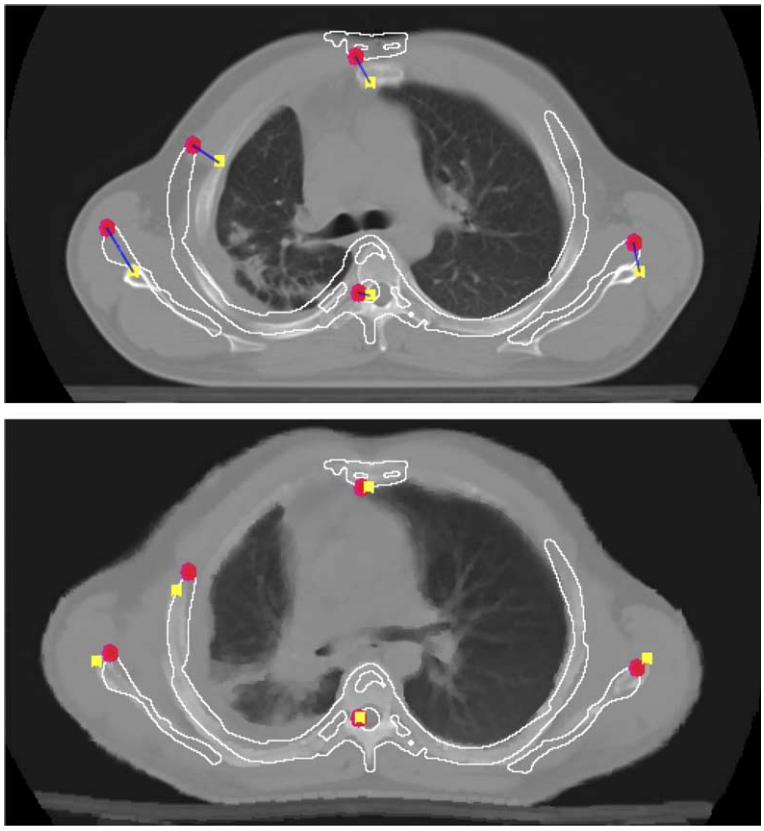

Fig. 5. Correspondence of interpolant points for a randomly selected lung CT transverse slice for Patient-11 of Group B. Top image: vertebrae, ribs and blades contours of the reference transverse slice superimposed on the float slice at the same z-coordinate, before nonrigid registration. The circular points belong to the reference slice while the rectangular ones to the float slice. The visualized interpolant points lie *exactly* on the corresponding slices. Bottom image: vertebrae, ribs and blades contours of the reference transverse slice superimposed on the deformed float slice at the same z-coordinate, after the application of the nonrigid registration scheme.

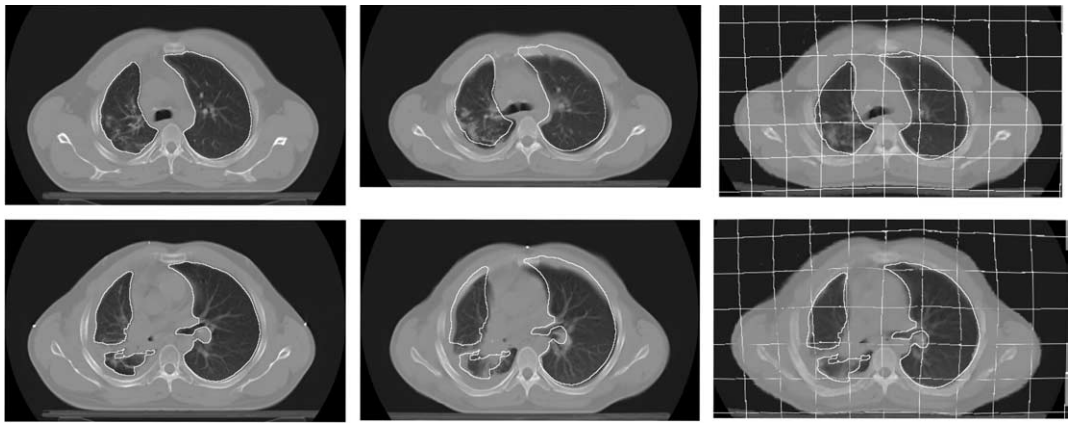

Fig. 6. Demonstration of the automatic elastic registration scheme based on the interpolant points for typical corresponding slices of Patient 11 of Group B by overlaying the lung contours of the reference data: reference slices (left images), float slices, before registration (middle images), deformed slices, after elastic registration (right images). The x- and y-coordinates of the displacement field are visualized in the form of a deformed wire frame, on the right images.

form with sufficient accuracy. Thus, an experienced radiologist manually segmented the tumor contour in all CT datasets and then a triangulation process is performed using the modified Marching Cubes algorithm (Delibasis et al., 2001) to reconstruct the tumor surface. The same procedure was applied for all CT datasets, reference, float (without elastic registration) and deformed (after elastic registration) sets, respectively. In Fig. 7, the lung tumor surfaces are displayed in VRML 2.0 format, where the left surface corresponds to the tumor of the reference data, the middle to the float data, and the right to the deformed data. As it can be observed for the specific patient, the deformed tumor recovers any deformation, compared to the float tumor volume (reduction of 8% in respect to the reference volume), and it resembles the reference tumor surface with a reduction of 35% of the volume due to radiotherapy treatment. Thus, the majority of the deformations occurred during acquisition can be recovered by the application of the proposed elastic registration scheme.

Furthermore, the performance of the SOM application, in finding correct correspondence between surface points of two CT sets, is mainly influenced by the two parameters: the window size, for the lateral interactions between the winning and the neighboring neurons, and the number of iterations. In Fig. 8, the number of surface points successfully corresponded by the application of the SOM network is displayed against changes of the window size (upper figure) and the number of iterations (lower figure) for a patient data. It can be seen that a size of 3×3 window is finally selected as it results to a higher number of successful corresponding points (495 surface points) and less computational complexity (compared to a 5×5 size window with 500 corresponding points and to a 7×7 size window with 497 corresponding points). The number of iterations is kept the same. Also, a maximum number of 50,000 iterations are finally used giving the best results in terms of number of successful corresponding points (495 corresponding surface points). Further increment of the number of iterations does

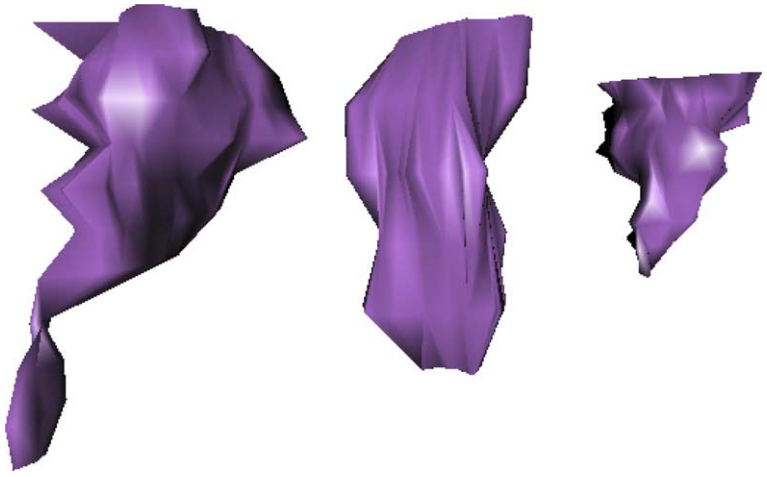

Fig. 7. Lung tumor surfaces for CT data of Patient-1 of Group A. Left: reference volume surface. Middle: transformed volume surface (before elastic registration). Right: deformed volume surface (after elastic registration).

not improve the performance of the SOM network. The total time of registration is approximately 9 min on a typical personal computer (Pentium IV, 768 RAM) distributed among the tasks as following: pre-registration: 1 min, determination of corresponding pairs of points: 0.5 min, application of elastic registration 7.5 min.

The performance of the proposed elastic registration scheme (called hereafter SOM-RBFs) is quantitatively assessed for completeness purposes, against the implementation of the surface registration based on the rigid transformation (called hereafter as surface-based registration). The performance of the SOM-RBFs method is compared to the simple rigid transformation using the average distance of the vertebrae, rib and shoulder blade contours as a common measure of match (MOM). The MOM is calculated be applying the transformation T under investigation (elastic or rigid) to the contours of the image to be transformed, which constitute set of points S_1, and calculate the average distance of the selected anatomical feature contours between the contours of the float image and the contours of the reference image (equivalently set of points S_2), using the DM of S_2. The DM is the result of the distance transform and is an image of the same dimensions of its input binary image. Each voxel of the DM holds the value of distance from the closest non-zero voxel of the input binary image (Matsopoulos et al., 2003).

The aforementioned MOM can be mathematically formulated according to the formula:

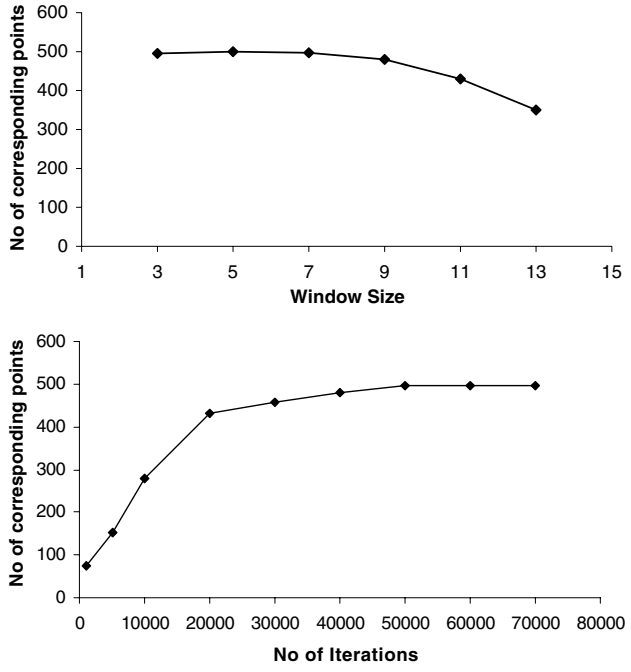

Fig. 8. Performance of the SOM network, in terms of the number of successful correspondence points, between surface points of the reference and transformed CT sets of a patient, against the window size and the number of iterations.

$$\mathrm{MOM} = \frac{1}{N} \sum_{(x_i, y_i, z_i) \in S_1} \mathrm{DM}(T(x_i, y_i, z_i)), \tag{11}$$

where N is the number of points in S_1 and $\mathrm{DM} = \mathrm{DT}(S_2)$.

In Table 1, the MOM for all patient data is calculated, in mm. The values of MOM for both methods are averaged over 10 independent executions for all image pairs to compensate for the stochastic (randomized) nature of the optimization method. It can be observed that the values of the average distance of the SOM-RBFs method are systematically lower than those of the surface-based registration method resulting an average MOM of around 6 mm for the early elastic method and around 11 mm for the later surface-based method, respectively. These findings confirm the application of a non-rigid registration method against a rigid-based method since the latter cannot recover the deformations occurred. Also, the values of the standard deviation indicate that the performance of the SOM-RBFs method is more consistent than the surface-based registration method (0.498 and 1.519 mm, respectively).

Finally, the lung tumor volumes (in %) in respect to the reference data (baseline examination corresponding to 100%) for all patients are shown in Fig. 9. According to this figure, the tumor volumes of the transformed data for each patient (CT data of each patient at an examination during the radiotherapy treatment) are initially calculated before the application of the elastic registration (white bars). To estimate the tumor volumes, an experienced radiologist traced the tumor contours at each slice delineating the gross tumor volume

Table 1
Average distance (MOM – in mm) for the all CT patient datasets by applying the SOM-RBFs algorithm and the surface-based registration method

Patient CT data	Measure of match (MOM) – average distance of extracted feature points (in mm)	
	Elastic matching scheme	Surface-based registration
	SOM-RBFs	Rigid transformation
Patient – 1	5.650	9.120
Patient – 2	6.340	11.345
Patient – 3	5.879	10.550
Patient – 4	6.760	12.455
Patient – 5	5.578	9.432
Patient – 6	6.768	12.756
Patient – 7	6.891	13.889
Patient – 8	5.762	10.378
Patient – 9	5.854	10.421
Patient – 10	6.078	11.798
Patient – 11	6.225	12.005
Patient – 12	5.776	11.228
Patient – 13	5.449	11.243
Patient – 14	5.995	11.134
Patient – 15	5.887	12.045
Average MOM	6.059	11.320
SD of MOM	0.450	1.251

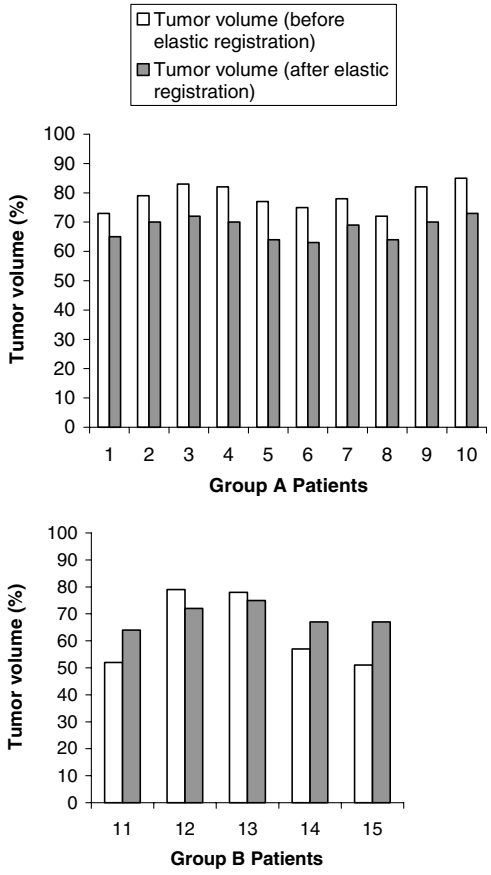

Fig. 9. Lung tumor volume (in %) with respect to the reference data of all patients of the Groups A and B, with and without the application of the elastic registration scheme. The white bars correspond to the volumes before registration while the grey bars to the volumes after elastic registration.

(GTV). Using a fill algorithm (Foley et al., 1996), the pixels enclosed in the contour are concerted into voxels by incorporating the slice thickness information. The number of these voxels is used as an estimate of the lung tumor volume. The application of the proposed elastic registration scheme results an estimation of the tumor volume (measured on the deformed CT data) since errors due to inspiration and/or movements have been eliminated by the elastic registration method (grey bars).

At this point it has to be mentioned that the observed tumor volume reductions, resulting from corrections after the application of elastic registration can be explained as follows for the two groups of patients: According to Fig. 9, the tumor volume correction resulting from elastic registration have a negative sign for all 10 patients of Group A. This was due to the fact that the measured tumor volume results from the initial tumor volume, which is affected by two factors: the irradiation during the period of four weeks and the physiologic movement effect. The first factor always reduces the volume, whereas the second factor, in the case of patients belonging to the Group A, tends to increase the volume due to instructions in terms of respiration, given to patients during image acquisition. Furthermore, at Group A, the expansion of the rib cage due to inspiration phase of the post-treatment CT (second factor) is expected and proven to be smaller than the shrinkage of the volume due to radiotherapy treatment (first factor). As it can be seen from the upper graph of Fig. 9, tumor volume corrections up to 8% were obtained for four patients, while corrections up to 12% were recorded for the rest patients; thus an average change of 11% in respect to each corresponding reference dataset were due to the physiologic movements for the patients of Group A.

In the case of patients of Group B, the elastically deformed tumor volume randomly fluctuates round the float data tumor volume, since no instructions, in terms of respiration, were given to the patients. Specifically, for the cases where the elastic correction increases the tumor volume of the float data, it is observed that the elastically pre-registered data were reduced to lower level than in patients of Group A. This is explained by the fact that the physiologic movement effect is added to the irradiation factor.

4. Discussion

In this paper, an automatic elastic registration scheme is proposed applied on thoracic CT data of patients diagnosed with NSCLC. The scheme includes the novel application of the SOMs in order to establish correspondence between automated segmented structures in conjunction with the implementation of a Radial Basis Function as a warping method. Results have shown that the elastic registration scheme can recover deformations occurred due to inspiration and/or any physiological movements. Furthermore, the proposed methodology has been compared against a surface-based registration method, using the rigid transformation, and quantitative results show its advantageous performance.

A key issue addressed to any point-based non-rigid registration method is the establishment of a correspondence between candidate surface points segmented from the data. In similar data registration applications, where motion and deformation of anatomical organs occur, such as registration of thoracic CT data (Betke et al., 2003) and registration of breast MR images with corresponding mammographic images (Behrenbruch et al., 2003), a neighborhood localization search method was used in conjunction with the ICP algorithm in order to obtain the closest correspondence between the surface points. Furthermore, the properties of point distinctiveness, point to point similarity, and point pair consistency have been incorporated into steps for the automatic extraction of corresponding point pairs of 2D medical images in order the parameters that define a transformation of one image onto the other to be estimated (Likar and Pernus, 1999). In our approach, the

correspondence between candidate surface points is established with the novel application of SOMs.

According to the proposed methodology, a Kohonen neural network is initialized to establish correspondence between surface points segmented from the reference and transformed sets. The application of the Kohonen model for automatic determination of the correspondence of surface points expands the idea described in (Fritzke, 1995; Camp et al., 1998) for surface triangulation. Using a 2D implementation of a Kohonen network, adjacent surface points in $\Re^3$ are mapped to adjacent neurons of the network by setting the neurons' weight vectors equal to the points Cartesian coordinates. The problem of automatic corresponding point determination can then be formulated as one of adapting the SOM associated with the set of points from the float image, using the extracted set of points from the reference image. After successful adaptation, a one-to-one correspondence between these points that coincide with the SOM weight vectors at the initial state is readily obtainable. Automation of approach, preservation of surface topology, selectable number of corresponding points, equal distribution and one-to-one point correspondence are the substantial advantages of the proposed technique. Nevertheless, it has to be pointed out that the paper is mainly focused on the introduction of SOMs towards the definition of automatic point correspondence rather than comparing methodologies with other existing ones. A future study must be carried out comparing methodologies for automatic point correspondence.

Crucial aspects that may affect the performance of a registration scheme applied on data under motion, like thoracic CT data, are the appropriate selection of the candidate corresponding points and the selection of the transformation that captures the true geometry of the lungs. In (Murphy et al., 2002), four fiducials have been implanted to each lung tumor in order the motion of the tumors to be recorded. This technique cannot be applicable for registering lung data in a routine clinical environment. In (Betke et al., 2003), 2D anatomical common structures such as the trachea, sternum and spine have been used as templates in order an initial registration to be achieved slice by slice. Then, a surface-based registration was applied by segmenting the lung surfaces. The performance of the initial registration based on these 2D common structures much depends on the protocol for acquiring the data; thus this detection method does not guarantee that the corresponding points are the same physical points, as it was also pointed out by the authors. Also, in (Betke et al., 2003), even though the initial alignment seems to work satisfactory with these structures, lateral chest structures, like the ribs, and/or 3D structures may be the solution to more accurate results in all image planes. In (Li et al., 2003) and (Fan et al., 2001), matching of airway brunch points, used as landmarks, were performed. The matching process was performed manually, limiting the usage of the whole registration method and also it cannot be applicable in cases where the lung tumor covers the lung area, as with the cases that are examined in the present paper. In our approach, the selection of candidate points was done in order firstly to be easily distinguished from the background, secondly to be paired so that accurate deformation information of the current point is available and thirdly to be uniformly distributed within the data. Vertebral spine, thoracic ribs and shoulder blades have been used as 3D common structures in the proposed elastic registration scheme, after they have been automatically segmented slice by slice. Furthermore, the selection of 3D points originated from these structures reduces inaccuracies introduced during registration since they are better approximate the same physical points.

In terms of transformation employed for the thoracic registration, in (Betke et al., 2003), a rigid transformation has been applied in order to globally register the lung CT data. Affine transformations were also employed in (Murphy et al., 2002, 2003). These transformations seemed to work satisfactory for these specific applications, where breath-holding of the patient and fast helical CT images have been used. Additionally, other researchers argue that non-rigid registration are the most suitable to recover the lung motion mainly due to the respiration (Rohr, 2000; Rohr et al., 2003). In the present study, a radial basis function, using the shifted log function, has been employed for the elastic registration of the lung CT data. This deformation model provides the advantage of coping with local deformations against the TPS method, which yields minimal bending energy properties measured over the whole image (Fornefett et al., 2001). To cope with local deformations, the landmarks used in the proposed registration scheme were well distributed over the image to prevent deformations in regions where no change is desired. Finally, the quantitative results by comparing the proposed elastic method against a widely used surface-based registration methods using the rigid transformation confirmed that the application of non-rigid registration is more suitable for the case of registering thoracic CT data where deformations occurred due to inspiration.

During the 3D implementation of the proposed warping method, two parameters must be considered: the choice of the g-function and the introduction of the bending factor λ. In the proposed implementation, the shifted log function has been selected as the g-function. Alternatively, the Gaussian g-function, $g(t) = \exp(t^2/\sigma^2)$ for $\sigma > 0$ may also be used, despite its strong locality effect, although further experimentation of the value of the standard deviation σ could resolve this issue.

The bending factor λ is an important parameter of the proposed elastic deformation method as it controls the degree of the total image warping (Rohr et al.,

2001). A constant value of λ has been selected during the registration of all lung CT datasets and it has been obtained experimentally. Alternatively, it is possible to selected different values of λ for each interpolant point. By allowing the bending factor λ to vary, a weighted warping could be obtained which will capture local deformities of specific areas of interest whereas relaxing the requirement for exact interpolant point matching in the rest of the image. Future experimentation with varying parameters of the λ could contribute to a more objective interpretation of the elastic registration method as well as to a quantitatively analysis of the information combined.

Another advantage of applying an elastic registration scheme on lung CT data is the estimation of tumor volume changes during radiotherapy treatment for all patients. It is well documented that lung tumors are difficult to be visualized at different sessions due to the movement of lesions located near the lung tumor area (Shimizu et al., 2000). In our experiments, changes of the tumor volume in respect to each reference dataset was found for all patients, which indicate inspiration and/or movement of the patient during acquisition of the data. Thus, the practical implementation of this scheme could provide estimations of lung tumor volumes since the scheme recovers these volumes from any added errors due to inspiration or any other movement of the patient. The usefulness of these findings in terms of a radiotherapy treatment planning system for the redesign of the treatment at different stages of the radiotherapy, remain to be explored.

Our ongoing effort in this research is aimed at developing a more robust registration framework in the context of larger and more diverse validation study. In the near feature, we intend to enhance the proposed non-rigid registration scheme with the combination of anatomical structure-based and intensity-based methods, the investigation of similarity measures, and/or the integration of uncertainties and error information.

References

Adams, R., Bischof, L., 1991. Seeded region growing. IEEE Trans. Pattern Anal. Machine Intell. 16, 641–647.

Arad, N., Dyn, N., Reisfeld, D., Yeshurun, Y., 1994. Image warping by radial basis functions: Application to facial expressions. J. Comput. Vis. Graphics Imag. Process. 56, 161–172.

Audette, M.A., Ferrie, F.P., Peters, T.M., 2000. An algorithmic overview of surface registration techniques for medical imaging. Med. Image Anal. 4, 201–217.

Behrenbruch, C.P., Marias, K., Armitage, P.A., Yam, M., Moore, N., English, R.E., Clarke, J., Brady, M., 2003. Fusion of contrast-enhanced breast MR and mammographic imaging data. Med. Image Anal. 7, 311–340.

Betke, M., Hong, H., Thomas, D., Prince, C., Ko, G.P., 2003. Landmark detection in the chest and registration of lung surfaces with an application to nodule registration. Med. Image Anal. 7, 265–281.

de Boer, J.C.J., van Sorensen de Koste, J.R., Senan, S., et al., 2001. Analysis and reduction of 3D systematic and random setup errors during the simulation and treatment of lung cancer patients with CT-based dose planning. Int. J. Radiat. Oncol. Biol. Phys. 49, 857–868.

Bookstein, F.L., 1989. Principal warps: thin-plate splines and the decomposition of deformation. IEEE Trans. PAMI. 11, 567–585.

Brown, M.S., McNitt-Gray, M.F., Goldin, J.G., Suh, J.W., Sayre, R.D., Aberle, D.R., 2001. Patient-specific models for lung nodule detection and surveillance in CT images. IEEE Trans. MI 20, 1205–1208.

Burns, J., Haramati, L.B., Whitney, K., Zelefsky, M.N., 2004. Consistency of reporting basic characteristics of lung nodules and masses on Computed Tomography. Acad. Radiol. 11, 233–237.

Cai, J., Chu, J.C.H., Recine, D., Sharma, M., Nguyen, C., Rodebaugh, R., Saxena, V.A., Ali, A., 1999. CT and PET lung image registration and fusion in radiotherapy treatment planning using the chamfer-matching method. Int. J. Radiat. Oncol. Biol. Phys. 43, 883–891.

Camp, J., Cameron, B., Blezek, B.D., Robb, R., 1998. Virtual reality in medicine and biology. Future Generat. Comput. Systems 14, 91–108.

Carcassoni, M., Hancock, E.R., 2001. An improved point proximity matrix for modal matching. In: International Conference on Pattern Recognition (ICPR'00), vol. 2, p. 2034.

Chamarthy, P., Stanley, R.J., Cizek, G., Long, R., Antani, S., Thoma, G., 2004. Image analysis techniques for characterizing disc space narrowing in cervical vertebrae interfaces, Comput. Med. Imag. Graph., 28, 39–50.

Delibasis, K.K., Matsopoulos, G.K., Mouravliansky, N., Nikita, K.S., 2001. A novel and efficient implementation of the Marching Cubes Algorithm. Comput. Med. Imag. Graph. 25, 343–352.

Engelsman, M., Damen, E.M.F., De Jaeger, K., et al., 2001. The effect of breathing and set up errors on the cumulative dose to a lung tumor. Radiother. Oncol. 60, 95–105.

Fan, L., Chen, C.W., Reinhardt, J.M., Hoffman, E.A., 2001. Evaluation and application of 3D lung warping and registration model using HRCT images. In: Proceedings of SPIE Medical Imaging, San Diego.

Foley, J.D., van Dam, A., Feiner, S.K., Hughes, J.F., 1996. Computer Graphics: Principles and Practice. Addison-Wesley, MA.

Fornefett, M., Rohr, K., Stiehl, H.S., 2001. Radial basis functions with compact support for elastic registration of medical images. Imag. Vis. Comput. 19, 87–96.

Fritzke, B., 1995. A growing neural gas network learns topologies. In: Tesauro, G., Touretzkt, D., Leen, T. (Eds.), Advances in Neural Information Processing Systems 7. MIT Press, Cambridge, MA, pp. 625–632.

Gee, J., Sundaram, T., Hasegawa, I., Uematsu, H., Hatabu, H., 2003. Characterization of regional pulmonary mechanics from serial magnetic resonance imaging data. Acad. Radiol. 10, 1147–1152.

Guest, E., Berry, E., Baldock, R., Fidrich, M., Smith, M., 2001. Robust point correspondence applied to two-and three-dimensional image registration. IEEE Trans PAMI. 23, 165–179.

Huang, J., Shimizu, H., Shioya, S., 2003. Clustering gene expression pattern and extracting relationship in gene network based on artificial neural networks. J. Biosci. Bioeng. 96, 421–428.

Hu, S., Hoffman, E.A., Reinhardt, J.M., 2001. Automatic lung segmentation for accurate quantification of volumetric X-ray CT images. IEEE Trans. MI 20, 490–498.

Jemal, A., Murray, T., Samuels, A., Ghafoor, A., Ward, E., Thun, M.J., 2003. Cancer Statistics, 2003. CA: A Cancer Journal for Clinicians 53, 2–55.

Kohonen, T., 1982. Self organized formation of topologically correct feature maps. Biol. Cybern. 43, 59–69.

Kohonen, T., 1989. Self-organization, and associative memory. Springer Verlag, Berlin.

Kozinska, D., Tretiak, O.J., Nissanov, J., 1997. Multidimensional alignment using Euclidean distance transform. Graph. Modell. Imag. Process. 59, 373–387.

Kubo, H.D., Hill, B.C., 1996. Respiratory gated radiotherapy treatment: A technical study. Phys. Med. Biol. 41, 83–91.

Kubo, M., Yamamoto, M.T., Kawata, Y., Niki, N., Eguchi, K., Ohmatsu, H., Kakinuma, R., Kaneko, M., Kusumoto, M., Moriyama, N., Mori, K., Nishiyama, H., 2001. CAD system for the assistance of comparative reading for lung cancer using serial helical CT images. In: Niessen, W.J., Viergever, M.A. (Eds.), Medical Image Computing and Computer-Assisted Intervention–MICCAI 2001, Fourth International Conference, Utrecht, The Netherlands. Springer Verlag, Berlin, pp. 1388–1390.

Lagerwaard, F.J., Van Sorensen De Koste, J.R., Nijssen-Visser, M.R.J., Schuchhard-Schipper, R.H., Oei, S.S., Munne, A., Senan, S., 2001. Multiple "Slow" CT scans for incorporating lung tumor mobility in radiotherapy planning. Int. J. Radiat. Oncol. Biol. Phys. 51, 932–937.

Li, B., Christensen, G.E., Hoffman, E.A., McLennan, G., Reinhard, J.M., 2003. Establishing a normative atlas of the human lung. Acad. Radiol. 10, 255–265.

Likar, B., Pernus, F., 1999. Automatic extraction of corresponding points for the registration of medical images. Med. Phys. 26, 1678–1686.

Lin, K., Yang, M., Liu, H., Lirng, J., Wang, P., 2003. Generalized Kohonen's competitive learning algorithms for ophthalmological MR images segmentation. Magnet. Reson. Imag. 21, 863–870.

Maintz, J.B.A., Viergever, M.A., 1998. A survey of medical image registration. Med. Image Anal. 2, 1–36.

Magnotta, V.A., Bockholt, H.J., Johnson, H.J., Christensen, G.E., Andreasena, N.C., 2003. Subcortical, cerebellar, and magnetic resonance based consistent brain image registration. NeuroImage 19, 233–245.

Makela, T., Clarysee, P., Lotjonen, J., Sipila, O., Lauerma, K., Hanninen, H., Pyokkimies, E.P., Nenonen, J., Knuuti, J., Katila, T., Magnin, I.E., 2001. A new method for the registration of cardiac PET and PR images using deformable model based segmentation of the main thorax structures. In: Niessen, W.J., Viergever, M.A. (Eds.), Medical Image Computing and Computer-Assisted Intervention–MICCAI 2001, Fourth International Conference, Utrecht, The Netherlands. Springer Verlag, Berlin, pp. 557–564.

Markey, M.K., Lo, J.Y., Tourassi, G.D., Floyd Jr., C.E., 2003. Self-organizing map for cluster analysis of breast cancer database. Artific. Intell. Med. 27, 113–127.

Matsopoulos, G.K., Marshall, S., 1994. Use of morphological image processing techniques for the measurement of a fetal head from ultrasound images. Pattern Recogn. 27, 1317–1324.

Matsopoulos, G.K., Delibasis, K.K., Mouravliansky, N.A., 2001. Medical image registration and fusion techniques: A review. In: Stergiopoulos, Stergios (Ed.), Advanced Signal Processing Handbook – Theory and Implementation for Radar, Sonar, and Medical Imaging Real-Time Systems. CRC Press, Boca Raton, FL, pp. 19.1–19.30 (Chapter 19).

Matsopoulos, G.K., Delibasis, K.K., Mouravliansky, N.A., Asvestas, P.A., Nikita, K.S., Kouloulias, V.E., Uzunoglu, N.K., 2003. CT-MRI automatic surface-based registration schemes combining global and local optimization techniques. Technol. Health Care: Official Journal of the European Society for Engineering and Medicine 11, 219–232.

Mayoral, R., Pérez-Ilzarbe, M.J., 2000. Competitive Hopfield neural network for stereo vision correspondence. In: IEEE-INNS-ENNS International Joint Conference on Neural Networks (IJCNN'00), vol. 5, p. 5464.

Movsas, B., Moughan, J., Komaki, R., Choy, H., Byhardt, R., Langer, C., Goldberg, M., Graham, M., Ettinger, D., Johnstone, D., Abrams, R., Munden, R., Starkschall, G., Owen, J., 2003. Radiotherapy patterns of care study in lung carcinoma. J. Clin. Oncol. 21, 4553–4559.

Murphy, M.J., Martin, D., Whyte, R., Hai, J., Ozhasoglu, C., Le, O.T., 2002. The effectiveness of breath-holding to stabilize lung and pancreas tumors during radiotherapy. Int. J. Radiat. Oncol. Biol. Phys. 53, 475–482.

Murphy, M.J., Chang, C.D., Gibbs, I.C., Le, Q.T., Hai, J., Kim, D., Martin, D.P., Adler, J.R., 2003. Patterns of patient movement during frameless image-guided radiosurgery. Int. J. Radiat. Oncol. Biol. Phys. 55, 1400–1408.

National Cancer Institute, 1994. SEER Cancer Statistics Review 1973–1991, National Institutes of Health, US Department of Health and Human Services. http://www.meds.com/lung/seer.html.

Oie, H.K., Gazdar, A.F., 1996. Initiation of cell cultures from lung tumors biopsies. In: Pass, H.I., Mitchell, J.B., Johnson, D.H., Turrisi, A.T. (Eds.), Cancer: Principles and Practice. Lippincott-Raven Publishers, Philadelphia, pp. 151–159.

Press, W.H., Teukolsky, S.A., Vetterling, W.T., Flannery, B.P., 1993. Minimization or maximization of functions. In: Numerical recipes in C: the art of scientific computing, second ed. Cambridge University Press, UK, pp. 412–420.

Rohr, K., 2000. Elastic registration of multimodal medical images: a survey. Künstliche Intelligenz. 3/00, 11–17.

Rohr, K., Stiehl, H.S., Sprengel, R., Buzug, T.M., Weese, J., Kuhn, M.H., 2001. Landmark-based elastic registration using approximating Thin-Plate Splines. IEEE Trans. MI. 20, 526–534.

Rohr, K., Fornefett, M., Stiehl, H.S., 2003. Spline-based elastic image registration: integration of landmark errors and orientation attributes. Comput. Vis. Imag. Under. 90, 153–168.

Ross, C.S., Hussey, D.H., Pennington, E.C., et al., 1990. Analysis of movement of intrathoracic neoplasms using ultrafast computerized tomography. Int. J. Oncol. Biol. Pgys. 18, 671–677.

Rueckert, D., Sonoda, L.I., Hayes, C., Hill, D.L.G., Leach, M.O., Hawkes, D.J., 1999. Nonrigid registration using free-form deformations: application to breast MR images. IEEE Trans. MI. 18, 712–721.

Serra, J., 1988Image Analysis and Mathematical Morphology, vol. 2. Academic Press, New York.

Shen, H., Fan, L., Qian, J., Odry, B.L., Novak, C.L., Naidich, D.P., 2002. Real-time and automatic matching of pulmonary nodules in follow-up multi-slice CT studies. In: Proceedings of the International Conference on Diagnostic Imaging and Analysis. Shanghai, China, pp. 101–106.

Shimizu, S., Shirato, H., Kagei, K., et al., 2000. Impact of respiratory movements on the computed tomographic images of small lung tumors in three-dimensional (3D) radiotherapy. Int. J. Radiat. Oncol. Biol. Phys. 46, 1127–1133.

Wolberg, G., 1998. Image morphing: a survey. The Visual Computer 14, 360–372.

The World Health Organization, 1982. Histological typing of lung tumors. Am. J. Clin. Pathol. 77, 123.

Wismuller, A., Meyer-Base, A., Lange, O., Auer, D., Reiser, M.F., Summers, D., 2004. Model-free functional MRI analysis based on unsupervised clustering. J. Biomed. Inform., 37, 10–18.

Zana, F., Klein, J.C., 2001. Segmentation of vessel-like patterns using mathematical morphology and curvature evaluation. IEEE Trans Image Proc. 10, 1010–1019.